International Journal of Heat and Mass Transfer 51 (2008) 5511–5521

Contents lists available at ScienceDirect

International Journal of Heat and Mass Transfer

journal homepage: www.elsevier.com/locate/ijhmt

Bio-heat transfer analysis during short pulse laser irradiation of tissues

Megan Jaunich [a], Shreya Raje [a], Kyunghan Kim [b], Kunal Mitra [a,*], Zhixiong Guo [b]

[a] Mechanical and Aerospace Engineering Department, Florida Institute of Technology, Melbourne, FL 32901, USA
[b] Department of Mechanical and Aerospace Engineering, Rutgers, The State University of New Jersey, Piscataway, NJ 08854, USA

ARTICLE INFO

Article history:
Received 15 October 2007
Received in revised form 4 April 2008
Available online 10 June 2008

Keywords:
Short pulse laser
Tissue irradiation
Focused laser beam
Non-Fourier heat conduction

ABSTRACT

The objective of this paper is to analyze the temperature distributions and heat affected zone in skin tissue medium when irradiated with either a collimated or a focused laser beam from a short pulse laser source. Experiments are performed on multi-layer tissue phantoms simulating skin tissue with embedded inhomogeneities simulating subsurface tumors and as well as on freshly excised mouse skin tissue samples. Two types of lasers have been used in this study – namely a Q-switched pulsed 1064 nm Nd:YAG short pulse laser having a pulse width of 200 ns and a 1552 nm diode short pulsed laser having a pulse width of 1.3 ps. Experimental measurements of axial and radial temperature distribution in the tissue medium are compared with the numerical modeling results. For numerical modeling, the transient radiative transport equation is first solved using a discrete ordinates method for obtaining the intensity distribution and radiative heat flux inside the tissue medium. Then the temperature distribution is obtained by coupling the bio-heat transfer equation with either hyperbolic non-Fourier or parabolic Fourier heat conduction model. The hyperbolic heat conduction equation is solved using MacCormack's scheme with error terms correction. It is observed that experimentally measured temperature distribution is in good agreement with that predicted by hyperbolic heat conduction model. The experimental measurements demonstrate that converging laser beam focused directly at the subsurface location can produce desired high temperature at that location compared to that produced by collimated laser beam for the same laser parameters. Finally the ablated tissue removal is characterized using histological studies as a function of laser parameters.

1. Introduction

Laser interaction with tissues can be categorized into several mechanisms which include photo-thermal, photo-mechanical (or photo-acoustical), and photo-chemical [1,2]. A more recent area of study is the phenomenon of plasma-mediated ablation, sometimes called photo-ablation, which can be achieved using short pulsed lasers [3,4]. These four mechanisms can occur individually or in combination depending upon laser parameters. Amongst these mechanisms, the one most easily quantified and commonly observed is the photo-thermal effect. This effect can be achieved during laser–tissue interaction through high energy deposition and vaporization of water in the tissue. The Photo-thermal mechanism of tumor irradiation has been used for applications like laser-induced hyperthermia (HT) [5], laser-induced interstitial thermotherapy (LITT) [6] and interstitial laser photocoagulation therapy (ILP) [7] all of which involve localized heating of cancerous or tumor tissue. Hyperthermic treatment is often utilized in combination with other treatments such as chemotherapy in order to more effectively destroy tumor tissue than either treatment alone [8,9]. Interstitial laser-induced thermotherapy has been studied for the treatment of head and neck cancers [10,11] as well as liver cancer [11,12]. This treatment involves the destruction of tumors by directly heating them in situ as an alternative to some combination of surgery, radiation, and chemotherapy. Interstitial laser photocoagulation is a therapeutic technique for the ablation of tumors using a low power laser for an extended duration, on the order of 8–10 min and was originally reported by Brown in 1983 [13]. Optical fibers are often used for delivery of the laser light and enable patients to be treated without requiring a major surgical procedure. This technique has been studied for treatment of many tumors, including those of the liver, urinary tract, and breast with positive clinical outcomes [7,14,15].

Though majority of the tumor irradiation techniques use continuous wave (CW) or long pulsed laser, however, short pulsed lasers are recently being preferred for these applications [16]. The ability to produce highly localized heating at the desired location has made pulse laser more attractive for tumor irradiation than CW lasers. This is because for the same energy input, the instantaneous peak power attained during pulsed laser irradiation is greater than that obtained in CW laser irradiation [17].

It has been well established that the tissues are sensitive to the temperature rise. The thermal impact on tissue changes drastically

* Corresponding author. Tel.: +321 674 7131;fax: +321 674 8813.
E-mail address: kmitra@fit.edu (K. Mitra).

0017-9310/$ - see front matter © 2008 Elsevier Ltd. All rights reserved.
doi:10.1016/j.ijheatmasstransfer.2008.04.033

Nomenclature

c	speed of light
C_p	specific heat of tissue
C_b	specific heat of blood
f_D	focused depth
H	sample height
I	scattered diffuse intensity
I_c	collimated intensity
κ	thermal conductivity of tissue
k_a	absorption coefficient of tissue
k_e	extinction coefficient
k_s	scattering coefficient of tissue
L_0	maximum intensity
n	refractive index of tissue medium
q	heat flux
q^r	radiative heat flux
r, z	spatial coordinates
R	sample radius
R_D	beam radius at the focal plane
R_0	beam radius at the sample surface
S	source term
t	time
t_p	pulse width of laser beam
T	temperature
T_a	temperature in arterial blood
$u(t)$	unit step function

Greek symbols

α	thermal diffusivity of tissue
$\delta(t)$	Dirac delta function
μ, η, ξ	direction cosines
ρ	density of tissue
ρ_b	density of blood
τ	relaxation time
ω_b	blood perfusion rate
Φ	phase function
Ω	solid angle
ϕ	azimuthal angle
σ	standard deviation
σ_s	Stephan–Boltzmann constant

when the temperature rise exceeds 43 °C [18]. It has been found that peak temperature in the range of 60–80 °C is required to ensure complete tumor necrosis without any post-treatment trauma [19]. However, it has been also observed that temperature required to kill the tumor tissue depends on the exposure time [20,21]. Robinson et al [22] has predicted that temperature elevation to at least 56 °C for 1 s or more should be sufficient to kill cancer cells. Thus there is no general consensus in the literature about the exact extent of temperature rise and exposure time necessary for complete tumor ablation.

Adoption of proper beam delivery technique is very important to initiate photo-thermal or photo-ablative effects for complete destruction of tumor. Selection of proper beam delivery technique depends mainly on the location of the tumor in the body. If the tumors are located deep inside the body then fiber-optic delivery system is used to transport laser light to the tumor site [23,24]. These fibers deliver the beam either in the form of collimated beam or in the form of diffused beam. Due to the collimated or diffused nature of the beam as used in tumor irradiation therapies like laser-induced hyperthermia and LITT, high power and long exposure time is required to achieve the desired fluence. This often leads to significant heat spread damaging surrounding healthy tissues. Moreover, fibers are often inserted into the tumor site to achieve volumetric heating. The same technique of fiber-optic delivery of laser light is also used for irradiating subsurface tumors. However, for skin tumors or subsurface tumors this perforation of the skin can be eliminated if a converging laser beam focused at the subsurface location is used. It has already been demonstrated that depending on the wavelength of irradiation, depth of penetration during laser–tissue interaction can reach as deep as 1 cm [25]. However, if collimated or diffused beam is used, most of the energy gets absorbed by tissue at the skin surface.

The technique of focusing a laser beam at the treatment location using a converging lens can reduce the absorption of laser energy by the skin. Due to the concentration of energy in a focused beam, it can penetrate the skin and reach greater depths without significant attenuation. A theoretical study has already been performed demonstrating this significant increase in peak absorption at the focal plane [26]. As a result of peak absorption at the focal plane, a desired subsurface temperature higher than the surface temperature can be achieved. This technique has been used for applications such as Non-ablative Dermal Remodeling [27,28] and treatment of striated muscles [29]. In this paper, this technique of using converging laser beam focused at the subsurface tumor location is used to achieve desired temperatures within the tumor tissue while keeping the surface temperature under control.

A detailed understanding of bio-heat transfer phenomenon is required to design a new method which can ensure accurate and controlled deposition of energy into the exact location of biological tissues with minimum collateral thermal damage to adjoining healthy tissue during any laser therapy. Substantial efforts have been made previously to develop a complete theoretical model considering the inherent complexity of the heat transfer process in tissue medium. Traditional analysis of heat transfer by conduction in biological tissues is performed using Fourier's law. In Fourier's law, heat conduction is assumed to be an instantaneous process with an infinite speed of propagation of the thermal signal, indicating that a local thermal change causes an instantaneous perturbation in the temperature at each point in the medium, even if the intervening distances are very large. To consider a finite speed of propagation, damped wave models have been proposed which lead to a hyperbolic heat conduction equation [30] or dual phase lag (DPL) equation [31]. With the development of this damped wave model theory of heat diffusion, an important parameter called thermal relaxation time (τ) needs to be considered [31–34]. Thermal relaxation time is a material property which indicates the time required for the heat flux to adjust or relax to the changes in the temperature gradient. It has already been demonstrated that calculations of heat transfer processes which occur for time periods less than the relaxation time of the medium may yield incorrect results if the Fourier model is used for applications such as burning of skin subjected to instantaneous heating [35] and cryo-preservation of skin [36].

Comparison of results obtained from numerical modeling with the experimental measurements is of prime importance for designing efficient technique of thermal treatment of tumors. For the study of heat affected zone in skin tissue phantoms using collimated laser beam, experimental measurements have been compared with numerical modeling results obtained using one-dimensional Fourier heat conduction model [37] and two-dimensional axisymmetric hyperbolic heat conduction formulations [38]. The validity of the use of hyperbolic heat conduction formulation for the case of bologna meat samples when irradiated with a collimated laser beam from a short pulse or CW laser source has been also reported in the literature [38].

Most of the previous numerical works have modeled the laser source term in bio-heat transfer equation by either Lambert's law or diffusion approximation. The scattering effect is hardly incorporable in Lambert's law. The diffusion approximation is limited to predominant scattering medium. Such treatment can introduce significant error in radiation flux distribution in practical nonhomogeneous tissue medium [39] during short pulse laser irradiation, in which case light suffers significant scattering in most region and strong localized absorption in the target spot. Therefore, it is necessary to consider complete light transport through the tissue medium for analyzing bio-heat transport in tissues during short pulse laser irradiation.

Measurement of temperature rise in tissues during laser irradiation helps determine the size of the heat affected zone, but it does not show the extent of cellular damage produced during laser irradiation. A detailed histological study is therefore required to correlate energy input, temperature rise, and the extent of cellular damage. The ability to provide direct visual information of thermal damage produced by the laser made this technique essential for both fundamental and application oriented studies. Histological analysis of morphological changes has been used extensively to study the mechanism of tissue ablation [40–42] and tissue welding [43].

Various histological techniques, such as plastic embedding technique, paraffin embedding technique, and frozen section technique, have been used depending upon the type of tissue and resolution of the image required [44]. Among them, the frozen section technique is most commonly used in the study of therapeutic effects of lasers because of the simplicity of the technique and short processing time. The simplicity of the technique helps eliminate artifacts which are produced due to lengthy and extensive method of tissue processing as in the plastic embedding technique. Therefore, in this paper, the frozen section technique is used for histological analysis.

No study has been reported in the literature dealing with validation of experimental measurements with numerical models for the case of tissue irradiation using focused laser beam from a short pulse laser source. The current work focuses on comparing experimental and numerical axial and radial temperature distributions in single-layer phantoms and multi-layer tissue phantoms simulating skin which contains inhomogeneities that simulate a tumor and freshly excised mouse skin tissue samples. Skin tissue consisting of epidermis, dermis, and underlying muscles has different optical properties in each layer. The tissue samples are irradiated by a Q-switched Nd:YAG pulse laser and a 1552 nm diode short pulsed laser source which is focused directly at the inhomogeneity location in phantoms and at the surface or subsurface locations for the case of tissue sample using a converging lens. The effectiveness of using a focused beam rather than a collimated beam to obtain the required temperature rise at the region of interest with smaller heat affected zone is demonstrated. The experimental results are compared with the numerical results obtained using Pennes' bio-heat transfer equation coupled with either Fourier parabolic or non-Fourier hyperbolic heat conduction model. Results of multi-layer tissue phantoms are also compared with those of single-layer tissue phantom. Finally the ablated tissue removal is characterized using histological studies for different laser parameters.

2. Mathematical formulation

2.1. Mathematical model

The intensity redistribution inside the tissue medium as shown in Fig. 1 due to scattering of light in the tissue medium is obtained by solving the transient radiative transport equation [45,46]:

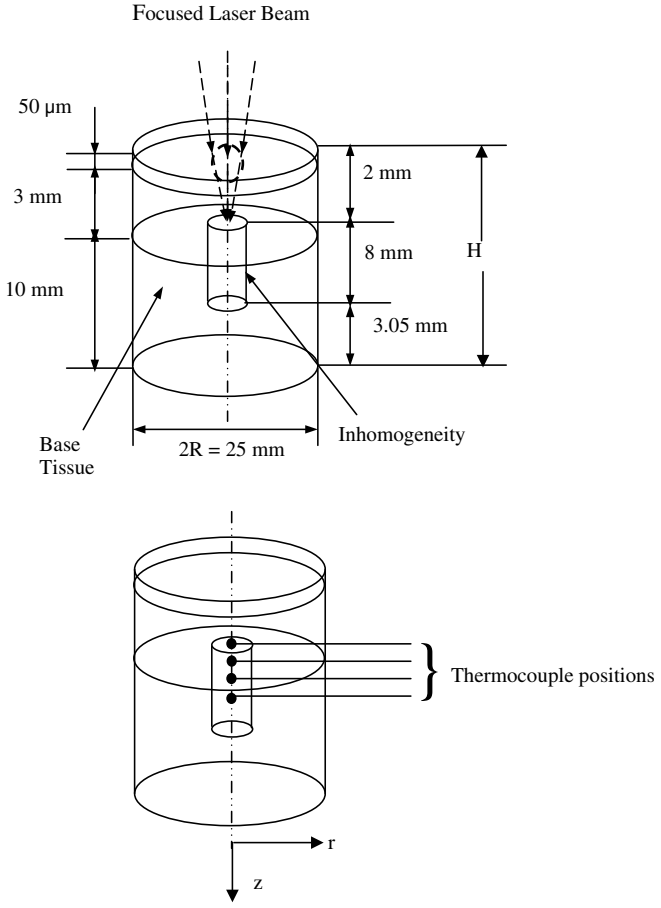

Fig. 1. Schematic of tissue phantom containing inhomogeneity.

$$\frac{1}{c}\frac{\partial I(r,z,\Omega,t)}{\partial t}+\frac{\mu}{r}\frac{\partial}{\partial r}[rI]-\frac{1}{r}\frac{\partial}{\partial \phi}[\eta I]+\xi\frac{\partial I}{\partial z}+k_e I = \frac{k_s}{4\pi}\int_{4\pi}\Phi(\Omega',\Omega)I(r,z,\Omega',t)\mathrm{d}\Omega+S(r,z,\Omega,t) \quad (1)$$

where I is the scattered diffuse intensity, k_e and k_s are the extinction coefficient and the scattering coefficient, respectively, ϕ is the azimuthal angle, Φ is the phase function, Ω is the solid angle, c is the velocity of light in the medium, r and z are the spatial coordinates, μ,η,ξ are direction cosines, t is the time, and S is the source term due from laser irradiation.

To calculate the source term S, the laser beam is assumed to be Gaussian in both the spatial and temporal domains and it is expressed as follows:

$$S(r,z,\Omega,t)=\frac{k_s}{4\pi}I_c(\mu^c\mu+\eta^c\eta+\xi^c\xi) \quad (2)$$

where the unit vector of (μ^c,η^c,ξ^c) represents the collimated laser incident direction. The collimated intensity I_c is given by

$$I_c(r,z,t)=L_0\exp\{-4\ln 2\times[(t-z/c)/t_p-1.5]^2\}\times\exp(-2r^2/\sigma(z)^2)\exp(-k_e z) \quad (3)$$

where L_0 is the maximum intensity of the laser beam at the sample surface, t_p is the laser pulse width, and $\sigma(z)$ is the beam radius varying with z for which the peak intensity drops to the e^{-2} value.

In the case of a converging laser beam as used in this paper which is focused at a depth of $z=f_D$, the standard deviation $\sigma(z)$ in Eq. (3) which varies with z can be expressed as follows:

$$\sigma(z) = \sigma(0)\left(\frac{-(R_0 - R_D)}{R_0}\frac{z}{f_D} + 1\right), \quad 0 \leqslant z \leqslant f_D$$
$$\sigma(z) = \sigma(0)\left(\frac{(R_0 - R_D)}{R_0}\frac{z}{f_D} - \frac{(R_0 - 2R_D)}{R_0}\right), \quad z > f_D \tag{4}$$

where $\sigma(0)$ is the standard deviation of radial intensity distribution at the sample surface, R_0 is the beam radius at the surface of the sample and R_D is radius of the beam at the focal plane.

Once the intensity distribution within the tissue medium is obtained using Eqs. (1)–(3), the corresponding temperature distribution is calculated by numerically solving Pennes' energy equation coupled with the proper heat conduction model. In this paper both Fourier parabolic heat and non-Fourier hyperbolic heat conduction models are considered.

Pennes' energy equation for the case of tissue medium has the following form:

$$-\nabla \cdot q(r,z,t) - \omega_b \rho_b C_b \rho[T(r,z,t) - T_a] - \nabla \cdot q^r(r,z,t) = \rho C_p \frac{\partial T(r,z,t)}{\partial t} \tag{5}$$

where ρ is the density of tissue, ρ_b is the density of blood, ω_b is blood perfusion rate, C_p is the specific heat of tissue, C_b is the specific heat of blood, T is the temperature, T_a is the temperature in arterial blood, q is the heat flux and q^r is the radiative heat flux. The term ω_b is set to zero if there is no blood perfusion as is the case for tissue phantoms and tissue samples.

The radiative heat flux can be expressed in terms of temperature using previously calculated intensity distribution in the following way:

$$\nabla \cdot q^r(r,z,t) = k_a\left(4n^2\sigma_s T^4 - \int_{4\pi} \Phi(\Omega',\Omega) I(r,z,\Omega',t)\mathrm{d}\Omega\right) \tag{6}$$

where n is refractive index of tissue medium and σ_s is Stephan–Boltzmann constant.

Heat flux due to conduction within the tissue medium can be expressed in terms of temperature distribution using either Fourier or non-Fourier heat conduction model. Heat conduction considering Fourier heat conduction model is expressed by following equation:

$$q(r,z,t) = -\kappa \nabla T(r,z,t) \tag{7}$$

where κ is the thermal conductivity of tissue and ∇ is the gradient operator.

The above parabolic diffusion equation implies an infinite speed of propagation of the thermal wave through the tissue medium. To eliminate this assumption of infinite speed of propagation of the thermal signal, a non-Fourier damped wave heat conduction model that takes into account finite speed of propagation of heat wave is considered and is given by [38,47–49]

$$q(r,z,t) + \tau \frac{\partial q(r,z,t)}{\partial t} = -\kappa \nabla T(r,z,t) \tag{8}$$

where τ is the relaxation time of the medium.

Eqs. (5)–(7) or 5,6,8 are simultaneously solved using suitable numerical scheme to obtain final temperature distribution as predicted by Fourier or non-Fourier heat conduction models, respectively.

The boundary conditions that are used are the following: (i) all the boundaries except the top laser incident surface are insulated, (ii) at the top surface convective heat exchange (convective heat transfer coefficient = 10 W/m^2 K) with surrounding ambient air (25 °C) is considered, (iii) the temperature profile is symmetric about the z-axis, and (iv) initially ($t = 0$) the temperature is equal to the ambient temperature and its derivative with respect time are zero everywhere in space. In the present tissue phantom model and tissue samples, the following simplifications are introduced: (1) radiation emission from the tissue phantom is neglected because the tissue blackbody intensity is much smaller than the incident laser intensity; (2) tissue optical and thermal properties are thermally stable during the heat transfer process; (3) blood perfusion and thermal evaporation and/or phase change of tissue during the heat transfer process are not considered.

2.2. Solution scheme

The transient discrete ordinates method (TDOM) with S_{10} scheme is employed for the solution of the transient radiation transfer equations given by Eqs. (1)–(3). To solve the hyperbolic heat conduction equations, MacCormack's predictor-corrector scheme is adopted. For information on the numerical schemes and accuracy validations, please refer to the recent publications of the co-authors [46,50]. Therefore, the details of the numerical methods are not repeated here. In the present calculations, a pulse train irradiation is considered and the heat conduction calculation starts following the temperature rise due to the first pulse incident. For layered-tissue phantoms, non-uniform grids are employed in order to capture precisely the heat transfer process.

3. Experimental methods

The schematic of the experimental set-up is shown in Fig. 2. Two types of lasers are used in this study: (1) a Q-switched short pulse Nd:YAG laser operating at a wavelength of 1064 nm and having a temporal pulse width (t_p) of 200 ns (FWHM) and (2) a 1552 nm desktop diode laser (Raydiance Inc.) operating at a wavelength of 1552 nm and having a temporal pulse width (t_p) of 1.3 ps (FWHM). For the Nd:YAG laser, the beam radius before the lens is 1 mm. The converging lens used for focusing the beam at the focal distance of 40 mm has a beam diameter of approximately 100 μm. For the case of 1552 nm laser the beam is focused using a high power 20× microscope objective which focuses the beam to a spot diameter of approximately 10 μm for a focal length of 21 mm. During the experiment the laser power is constantly monitored using a power meter. The samples are well insulated on all sides (except on the irradiated face) to prevent heat loss to the surroundings. A thermal imaging camera (IR Flexcam Pro, Infrared Solutions) is used to record the radial surface temperature profile of the samples. The images are recorded with computerized data acquisition system and processed with National Instruments IMAQ Vision Builder Image processing software. The camera provides a measurement range of 0–350 °C with a sensitivity of ±0.09 °C at 30 °C. The spectral response of the camera is 8–14 μm. For the axial temperature measurements in the tissue phantom, holes are drilled up to the central axis at discrete locations along the length of the phantom (see Fig. 1). T-type thermocouples having diameter of 0.5 mm are inserted into the holes for temperature measurements. Temperature readings of the thermocouples are recorded through a computerized data acquisition system using Labview Software. These thermocouples provide a measurement range from 0 °C to 480 °C with a sensitivity of ±1 °C and 0.2 s of response time.

Experiments are performed on both single-layer and three-layer tissue phantoms replicating skin layers and having an embedded inhomogeneity simulating tumors using Nd:YAG laser (Fig. 1). The phantoms are composed of araldite, DDSA (dodecenyl succinic anhydride) resin and DMP-30 (hardener) mixed in the ratio 1:0.87:0.04. Titanium dioxide particles (mean diameter = 0.3 μm) are added as a scatterer to the sample. India ink is used as the absorber. Details about phantom preparation can be found in the previous papers of the authors [51]. The layered-tissue phantom consists of three-layers having different optical properties representing epidermis, dermis, and fatty tissues of human skin. The

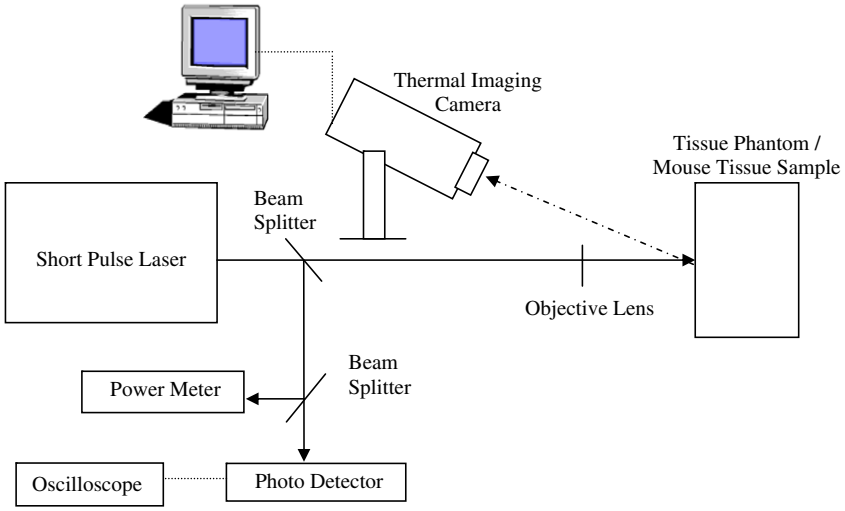

Fig. 2. Schematic of the experimental set-up for tissue irradiation using short pulse laser.

thickness, absorption coefficient (k_a), and scattering coefficient (k_s) of each layer of 1064 nm are tabulated in Table 1 [52,53]. For single-layer tissue phantom, the base tissue matrix has bulk average absorption coefficient (k_a) = 0.051 mm^{-1}, and scattering coefficient (k_s) = 6.14 mm^{-1}. These values are obtained by calculating weighted average of properties of different layers of layered-tissue phantom. The density (ρ) of the medium is 1000 kg/m^3, thermal conductivity (κ) is 0.35 W/m K, and the specific heat (C_p) is taken as 4200 J/kg K for all layers of tissue medium [35]. Inhomogeneities are drilled in tissue phantoms having scattering coefficient of 12.28 mm^{-1} and absorption coefficient of 0.051 mm^{-1}.

Experiments are also conducted with freshly excised skin tissue samples having thicknesses of 5–6 mm obtained from mice using both Nd:YAG and 1552 nm diode lasers. A typical tissue cross-section is 20 mm × 30 mm. The density (ρ), thermal conductivity (κ), and specific heat (C_p) are taken as 1000 kg/m^3, 0.35 W/m K, and 4200 J/kg K, respectively [54]. The thickness and optical properties of three different layers of the mouse skin tissues are presented in Tables 2 and 3 at wavelength of 1064 nm and 1552 nm, respectively [55].

After ablating the tissue with the laser, histological analysis is performed to analyze the damage zone produced by laser irradiation. The frozen sectioning technique is used for histological studies. The resolution provided by frozen section technique is sufficient to observe thermal damage in the tissue caused by laser irradiation. In this technique the ablated portion of the tissue is cut along with some surrounding non-irradiated tissue right after the ablation and embedded in the cryomold made of OCT (optimal cutting temperature) compound. Then sections of thickness 20 μm are cut using Cryostat. The temperature inside the Cryostat is maintained at −24 °C during sectioning. The sections are stained using Hematoxylin and Eosin (H&E) stain which is a rapid staining method that is commonly used due to its simplicity. This progressive stain creates stained sections which have deep blue nuclei with a pink or rose-colored background of other cytoplasmic structures. Once the sample preparation is complete, slides are viewed under an optical microscope using 40× magnification.

The ablation depth and width can be measured using image processing software (Scandium) in order to correlate ablation volume to laser parameters. The software is calibrated to provide measurements in millimeters corresponding to the magnification at which an image is captured. In this way, laser-induced damage volumes are calculated for a particular set of laser parameters.

4. Results and discussion

In this paper, temperature distributions in a tissue medium during a short pulse laser irradiation has been obtained both experimentally and numerically. Radial and axial temperature distributions are obtained in three-layer and single-layer tissue phantoms and in freshly excised tissue samples for the case of both collimated and focused laser beam using Nd:YAG laser. Experiments are also performed on freshly excised tissue samples using 1552 nm wavelength laser to obtain the radial temperature distribution. Numerical modeling results are obtained for both hyperbolic non-Fourier and parabolic Fourier case by solving a coupled set of equations consisting of the transient radiative transport

Table 1
Optical properties of different layers of human skin tissue at 1064 nm [52,53]

Layer	Thickness (mm)	Absorption coefficient (k_a) (mm^{-1})	Scattering coefficient (k_s) (mm^{-1})
Epidermis	0.05	0.355	8.237
Dermis	3	0.049	8.237
Fatty tissue	10	0.050	5.5

Table 2
Optical properties of different layers of mouse skin tissue at 1064 nm [55]

Layer	Thickness (mm)	Absorption coefficient (k_a) (mm^{-1})	Scattering coefficient (k_s) (mm^{-1})
Epidermis	0.05	0.7	8.0
Dermis	3	0.044	8.0
Fatty tissue	3	0.04	7.0

Table 3
Optical properties of different layers of mouse skin tissue at 1552 nm [55]

Layer	Thickness (mm)	Absorption coefficient (k_a) (mm^{-1})	Scattering coefficient (k_s) (mm^{-1})
Epidermis	0.05	1.00	12.5
Dermis	3	0.80	9
Fatty tissue	3	0.50	7.5

equation and Pennes' bio-heat transfer equation as discussed in previous section.

Experiments are performed on a three-layer inhomogeneous tissue phantom using a focused laser beam. The embedded inhomogeneous simulated tumor is drilled 2 mm underneath the phantom surface. For the case of the focused laser beam, the laser is focused directly at the inhomogeneity location ($z = 2$ mm) using a converging lens. It has already been discussed earlier that a temperature rise to approximately 43 °C is required for successfully irradiating tumors. Therefore, the sample is irradiated until 43 °C temperature rise is obtained at the focal plane, which is at the inhomogeneity location. The surface temperature is measured using a thermal camera and the temperature at $z = 2$ mm is measured using thermocouples.

It has been observed that the accuracy of prediction provided by hyperbolic heat conduction model depends on proper choice of thermal relaxation time (τ). The value of τ depends on the propagation velocity of thermal wave which is dependent on material structure and properties. Although its value has been measured for biological media such as bologna meat samples [33], the exact value of thermal relaxation time (typically having values in the range of 5–100 s) is unknown for most of the tissues. Fig. 3(a) shows radial temperature distribution at the inhomogeneity location, respectively, for the case of three-layer tissue phantom for different relaxation times (ranging from 10 s to 20 s). The results obtained using Fourier heat conduction model is also plotted. These numerically predicted results are compared with corresponding experimentally measured temperature distributions. The error bars plotted in the Fig. 3(a) represent uncertainty in experimental measurements. Considering a 99% confidence interval, the precision index for a total of three runs is calculated. The standard deviation between the three runs at each individual nodal point is evaluated. Thus the total uncertainty values at each nodal

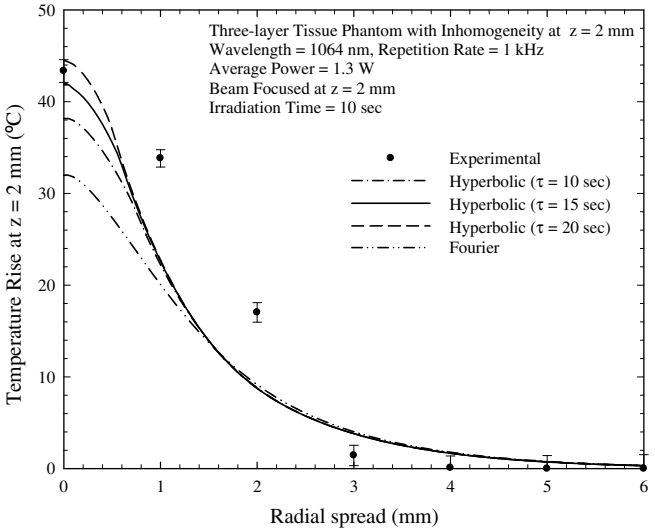

Fig. 3(a). Radial temperature distribution at the inhomogeneity location in a three-layer tissue phantom for different relaxation times.

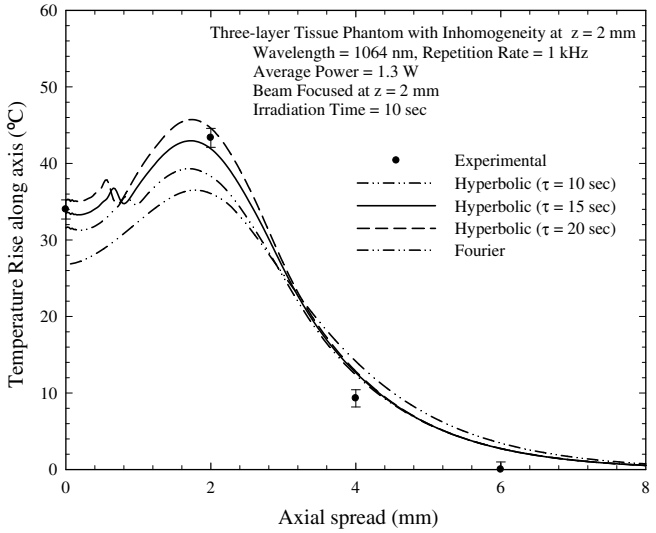

Fig. 3(b). Axial temperature distribution in a three-layer tissue phantom for different relaxation times.

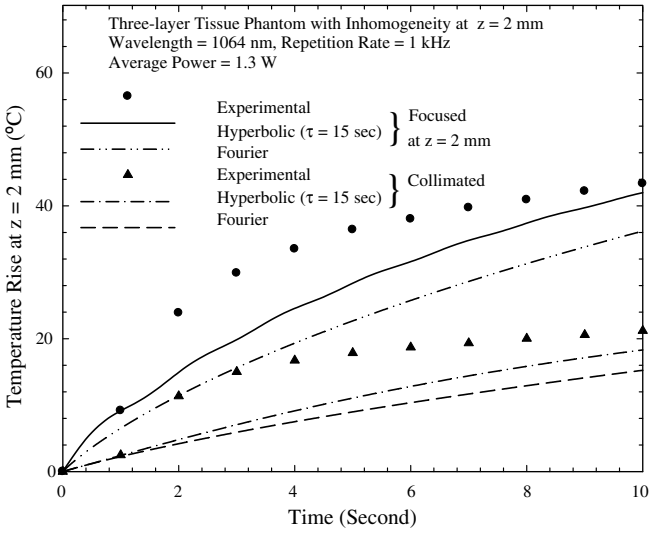

Fig. 4(a). Comparison of temperature history at the inhomogeneity location between collimated and focused laser beam irradiation for a three-layer tissue phantom.

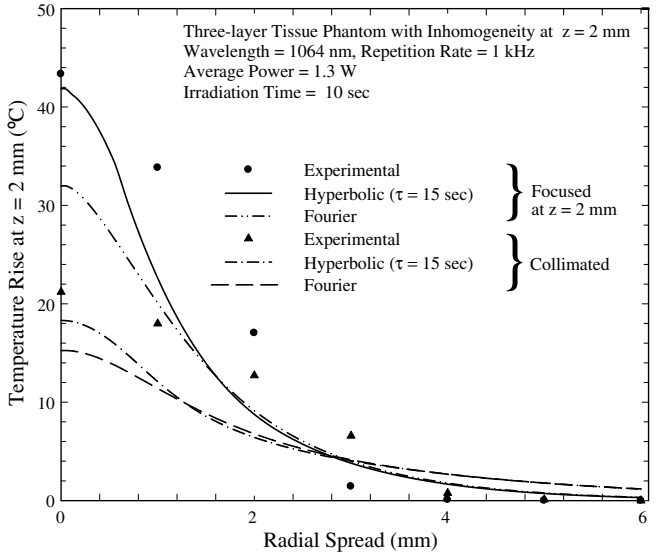

Fig. 4(b). Comparison of radial temperature distribution between collimated and focused laser beam irradiation for a three-layer tissue phantom containing inhomogeneity.

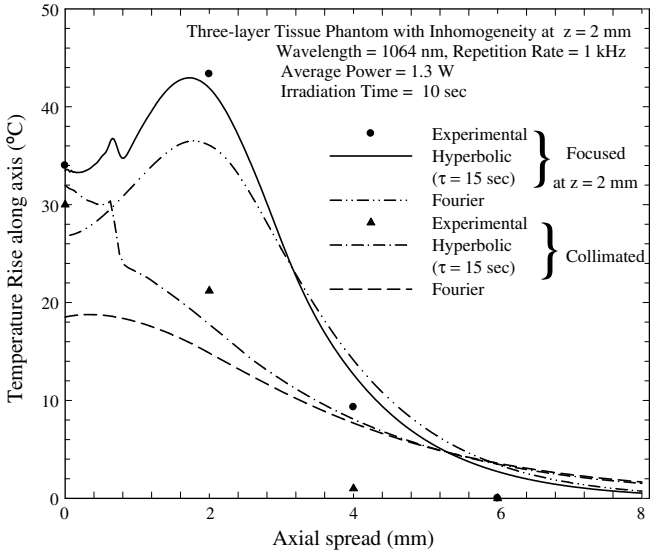

Fig. 4(c). Comparison of axial temperature distribution at the inhomogeneity location between collimated and focused laser beam irradiation for a three-layer tissue phantom.

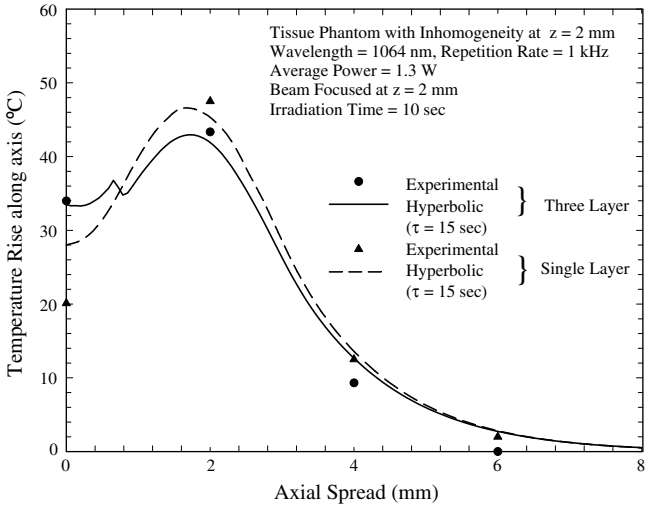

Fig. 5(b). Comparison of axial temperature distribution between a single-layer and a three-layer tissue phantom for focused laser beam irradiation.

point is the product of the precision index times the standard deviation. It is observed that a maximum total uncertainty of 1.5 °C is obtained for thermal camera and 1.2 °C for thermocouples. It is clear from Fig. 3(a) that for human skin tissue phantom, non-Fourier heat conduction model matches better with the experimental measurements for $\tau = 15$ s. On the other hand Fourier model predicts a significant lower temperature rise. Location of thermocouples at different radial locations used to measure radial temperatures may not be accurate and hence some deviation between experimental measurements and hyperbolic model is observed particularly for locations away from the laser beam axis. Corresponding axial temperature distribution along with error bars plotted in Fig. 3(b) also shows that hyperbolic heat conduction model for $\tau = 15$ s matches well with experimentally measured temperature distribution. This suggests that while studying heat transfer phenomena for a time scale shorter than the thermal relaxation time of the material, τ is one of the governing parameters. Without considering proper value of τ, bio-heat transfer models involving such analysis will produce erroneous temperature distributions. Therefore, for the case of tissue phantoms the value of τ is taken as 15 s.

Once selection of proper value of τ for the numerical model is accomplished, experiments are performed to demonstrate the advantage of using focused laser beam for subsurface tumor irradiation. Fig. 4(a) shows the temperature rise at the inhomogeneity location with time for both the cases of collimated and focused laser irradiation. The plot shows experimental data along with numerical modeling results obtained from hyperbolic heat conduction and Fourier heat conduction models. It is observed that converging laser beam focused at the subsurface location can produce much higher temperatures at that desired location compared to a collimated laser beam which is necessary for subsurface tumor irradiation. The deviation of experimental data from numerical modeling results is due to the limitation of placing the thermocouple at the exact location. Fig. 4(b) shows comparison of radial temperature distribution between experimental measurements and numerical modeling results obtained at inhomogeneity location (at z = 2 mm) for collimated and focused laser irradiation after

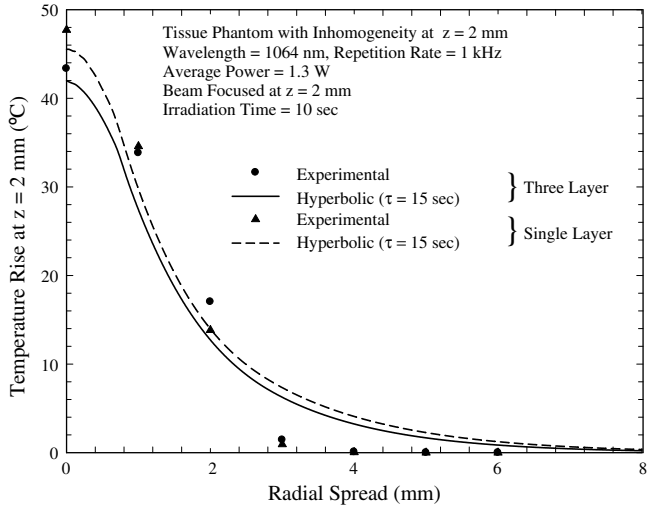

Fig. 5(a). Comparison of radial temperature distribution at the inhomogeneity location between a single-layer and a three-layer tissue phantom for focused laser beam irradiation.

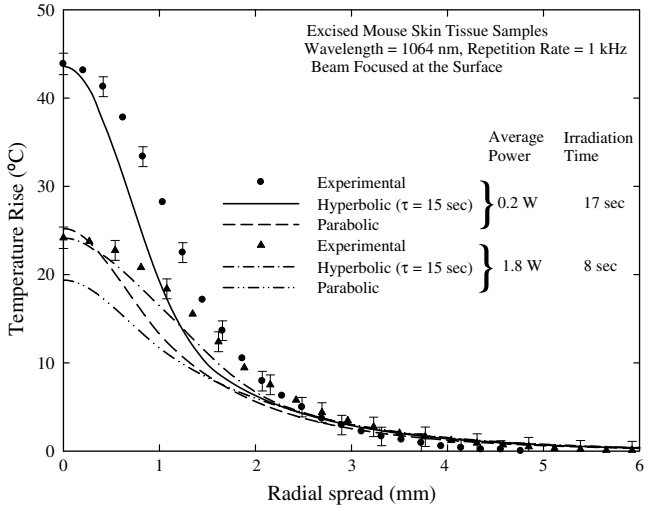

Fig. 6. Radial temperature distribution at the surface of freshly excised mouse skin tissue sample for different average powers for the case of 1064 nm, 200 ns laser.

10 s of laser exposure. It also emphasizes that focused beam is very effective in obtaining higher temperature rise below the surface at the desired location while keeping surface temperature comparatively lower thereby causing minimal thermal damage. On the contrary, collimated laser beam produces high temperature at the surface with a gradual decay of temperature along the depth. Corresponding axial temperature distribution is plotted in Fig. 4(c). In this figure, temperature distributions obtained from the hyperbolic heat conduction model shows a wave phenomenon. Experimental measurements could not capture this effect due to the limitation of placing thermocouples very close to each other (currently there is a separation distance of 2 mm between two consecutive thermocouples).

After demonstrating the advantage of using focused laser beam and performing model validation studies in a layered-tissue phantom, experiments are conducted to compare the temperature distribution between a single-layer and three-layer tissue phantoms. Conventionally, skin is treated as a single-layer medium for simplicity. But in reality, skin is a multi-layered medium having different thicknesses, scattering, and absorption coefficients in each layer (see Table 1). The goal of this part of the work is to investigate whether single-layer approximation of layered skin tissue is reasonable approximation or not. The radial temperature distribution at the inhomogeneity location ($z = 2$ mm) for the case of a single-layer tissue phantom is compared with that of a three-layer tissue phantom in Fig. 5(a). It is evident from figure that for the case of three-layer tissue phantom, the peak temperature rise is less but the radial heat spread is slightly more than that of single-layer tissue phantom. These differences can be attributed to the consideration of average optical properties throughout the whole tissue phantom in case of single-layer model. Also, axial temperature distribution (Fig. 5(b)) obtained from thermocouples placed at various depths of the phantom shows lower peak temperature rise (obtained at $z = 2$ mm) and smaller axial heat spread for three-layer tissue phantom. This is due to greater attenuation of laser beam caused by higher absorption coefficient of the first layer of three-layer tissue phantom as compared to single-layer tissue phantom. The top layer of the skin (epidermis) has high absorption coefficient which results in higher temperature rise at the surface in three-layer model than that of single-layer model. Also, a sharp temperature rise is observed for three-layer tissue phantom due to change in optical properties between first and the second layer. These results demonstrate that there is difference in heat affected zone in single-layer and three-layer model and hence skin should be modeled as a layered medium to analyze bio-heat transport phenomenon during short pulse laser irradiation of tissues.

After validating the numerical model for the case of tissue phantoms, experiments are next conducted on *in vitro* freshly excised mouse skin tissue samples. Tissue samples are prepared by excising the skin along with the adjoining muscle tissue from freshly sacrificed mouse. Tissue samples with muscle are irradiated by the laser beam focused at the surface. The temperature distribution at the surface of the tissue is measured using thermal camera. Numerical modeling results are obtained by considering the mouse skin tissue as a three-layer medium. Optical properties as a function of various layers of skin are taken from Table 2. Fig. 6 shows the experimentally measured surface radial temperature distribution along with corresponding numerical results obtained using Fourier parabolic heat conduction and non-Fourier hyperbolic heat conduction model for two different average powers. Error bars are plotted following the same procedure as previously described. Similar to phantom studies, experimental measurements match better with the results predicted by hyperbolic heat conduction formulation particularly the peak temperature rise at the laser incident spot. The Fourier model under-predicts the peak temperature

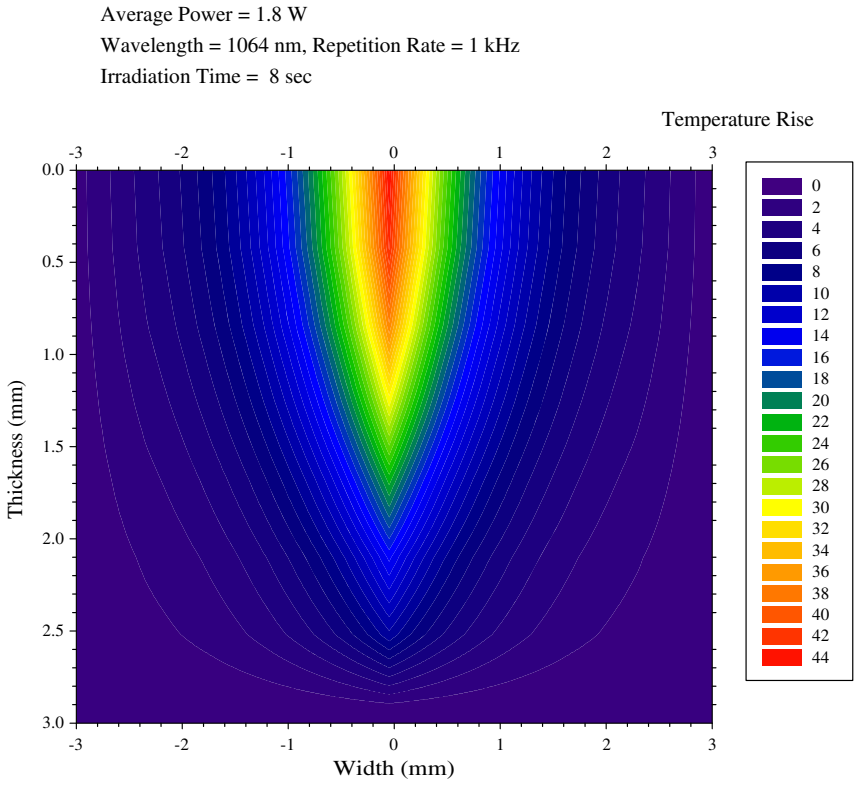

Fig. 7(a). Filled temperature contours obtained using the hyperbolic heat conduction model for the case of laser beam focused on the surface of excised mouse skin tissue sample.

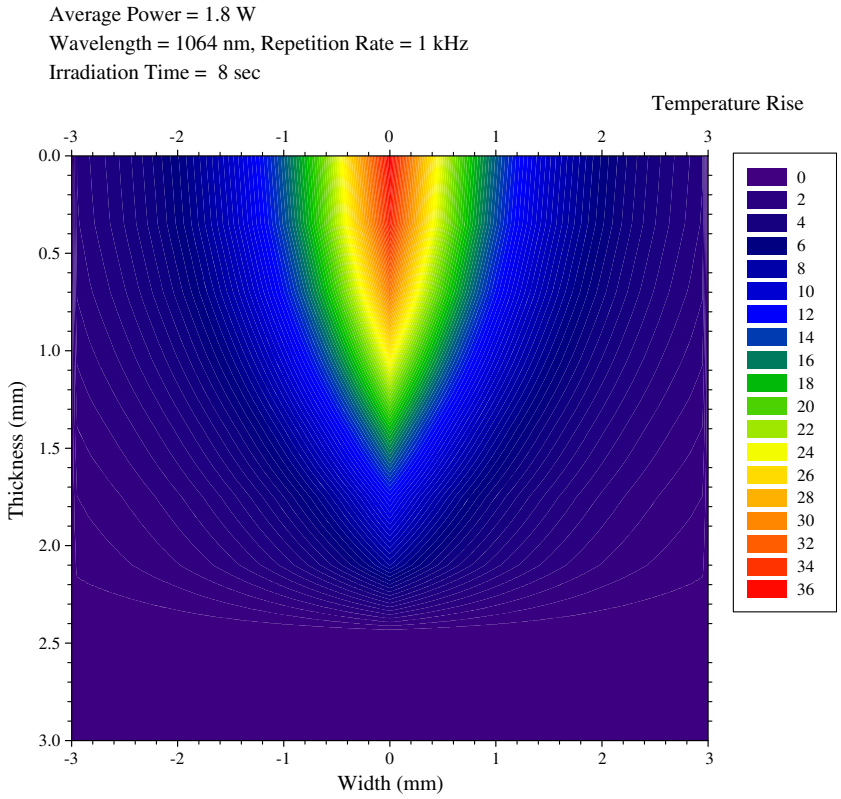

Fig. 7(b). Filled temperature contours obtained using Fourier heat conduction model for the case of laser beam focused on the surface of excised mouse skin tissue sample.

rise significantly. The reason for mismatch of experimental measurements with the numerical models can be attributed to the non-uniform thickness throughout the tissue sample cross-section. Numerical modeling results are obtained using a uniform tissue sample thickness. The filled temperature contours obtained using hyperbolic and Fourier heat conduction formulation are plotted in the Fig. 7(a) and 7(b) to highlight the difference in radial and axial temperature distribution predicted by two different heat conduction models for one such case (average laser power = 1.8 W). Assumptions of the diffusive nature of heat propagation in the Fourier heat conduction model produce larger radial heat spread with smaller penetration compared to that predicted by the hyperbolic heat conduction formulation.

Laser irradiation experiments are next performed on *in vitro* freshly excised mouse tissue samples using the 1552 nm laser. Fig. 8(a) and 8(b) shows temperature distributions for an average laser power of 1.3 W and 0.73 W along with repetition rate of 500 kHz and 250 kHz, respectively. For both cases, the beam is focused underneath the surface at $z = 1$ mm. Experimentally the surface temperature is measured using a thermal imaging camera and

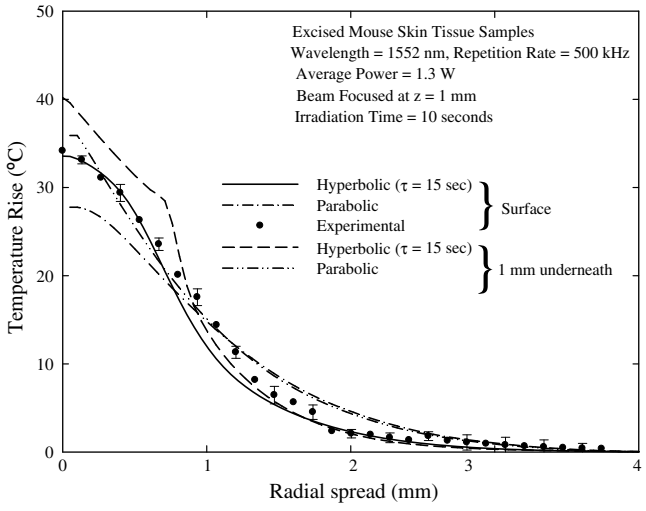

Fig. 8(a). Radial temperature distribution in freshly excised mouse skin tissue sample for beam focused at $z = 1$ mm for the case of 1552 nm, 1.3 ps laser having average power of 1.3 W.

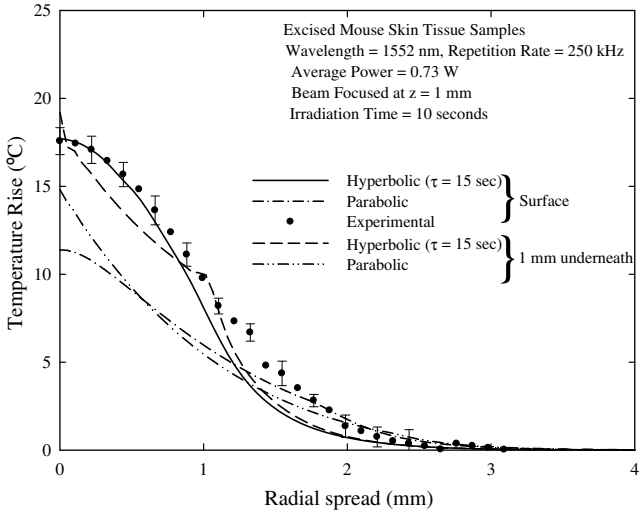

Fig. 8(b). Radial temperature distribution in freshly excised mouse skin tissue sample for beam focused at $z = 1$ mm for the case of 1552 nm, 1.3 ps laser having average power of 0.73 W.

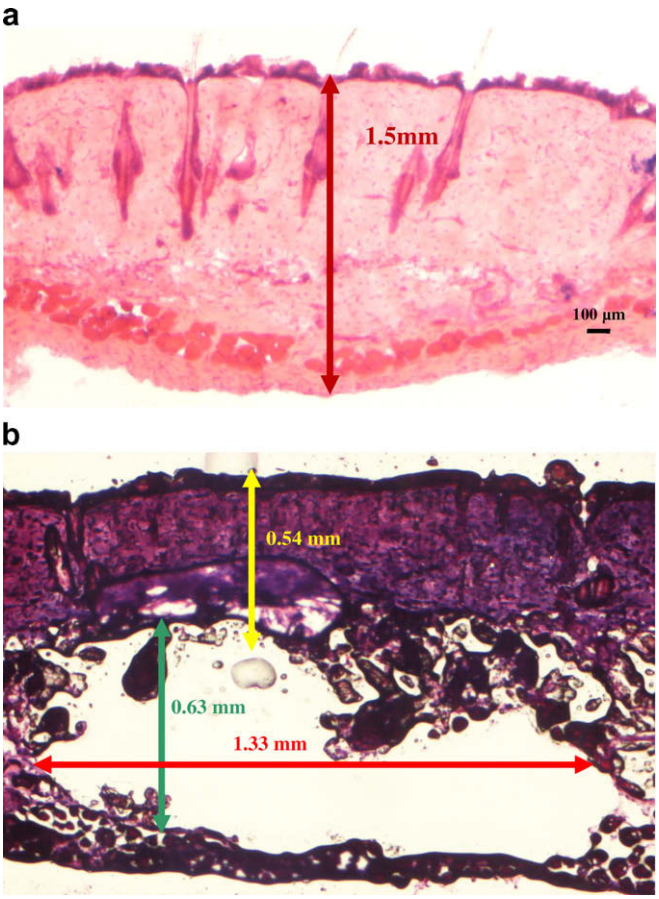

Fig. 9. Histological study of (a) freshly excised mouse skin tissue and (b) excised mouse tissue irradiated for 10 s for beam focused at $z = 1$ mm for the case of 1552 nm, 1.3 ps laser having average power of 1.3 W.

the results show very good agreement between the hyperbolic model and the experimental data. The Fourier model under-predicts the peak temperature rise. Numerical models are used to predict the temperature at subsurface locations ($z = 1$ mm) as it is not convenient to insert thermocouples accurately at such subsurface locations.

Fig. 9a and b show histological sections of non-radiated and laser irradiated mouse skin tissue, respectively. It is evident from the image in Fig. 9b that the region close to the skin surface remains intact where as the tissue is ablated by the laser beam at greater depths. Observation of Fig. 9b shows that for the case of the beam focused at $z = 1$ mm a clean subsurface ablated volume is obtained. However, for skin tissues interacting with a 1552 nm laser, the penetration depth of the beam into the tissue is found to be approximately 350 μm [2]. Beyond this penetration depth, the beam will get scattered in the tissue. The ablation area calculated by the interpolated polygon technique using processing software (Scandium) is found to be 0.64 mm^2. The large volume removal observed in Fig. 9b suggests that the beam scattering has contributed to the ablation. A difference in the shading of the two images is notable and is due to the gradual breakdown over time of the hematoxylin and eosin stains. Another cause of the color variation is imprecision in timing during the staining procedure.

5. Conclusion

In this work skin tissue is modeled as a layered medium to analyze heat transfer during collimated and focused laser irradiation. This study demonstrates that a converging laser beam focused at a subsurface location can produce a high temperature rise at the desired subsurface location while keeping the surface temperature low. The radial and axial temperature distributions obtained for multi-layer tissue phantoms during collimated and focused laser irradiation show that the focused beam can produce much more compact heat affected zone compared to that of collimated laser beams as traditionally used in most laser-based therapeutic applications. Experimental measurements are compared with numerical modeling results obtained from Fourier parabolic and non-Fourier hyperbolic heat conduction formulation for both human skin tissue phantom and mouse skin tissue sample. It is demonstrated that the hyperbolic heat conduction model is a more accurate model for such kind of analyses as it takes into account the relaxation time of the tissues. The Fourier parabolic heat conduction model, on the other hand, is found to deviate significantly from experimental measurements. This analysis emphasizes importance of considering a hyperbolic heat conduction formulation in studying heat transfer phenomenon for a time scale shorter than thermal relaxation time of the medium. The short pulse durations deliver high peak power to the target location which restricts the heat affected zone to a localized region. High laser intensity and short pulse laser duration can achieve significant ablated tissue removal with a range of collateral thermal damage. This effect can be reduced by scanning the tissue at a particular velocity over the desired region as compared to static ablation as performed in this study.

Acknowledgments

Kunal Mitra acknowledges partial support from Raydiance Inc. for this research. The authors will also like to acknowledge Prof. Michael S. Grace of Department of Biological Sciences for preparation of tissue samples.

References

[1] S.L. Jacques, Laser–tissue interactions: photochemical, photothermal, and photomechanical, Surg. Clin. N. Am. 72 (1992) 531–558.
[2] S.L. Jaques, How tissue optics affect dosimetry for photochemical photothermal and photomechanical mechanisms of laser–tissue interaction, Proc. SPIE (1991) 316–322.
[3] J.P. Fischer, J. Dams, M.H. Gotz, E. Kerker, F.H. Loesel, C. Messer, M.H. Suhm, J.F. Billie, Plasma-mediated ablation of brain tissue with picosecond laser pulses, Appl. Phys. B 58 (1994) 493–499.
[4] G. Muller, K. Dorschel, H. Kar, The tissue photoablation process with short pulsed Lasers, Proc. SPIE (1991) 150–177.
[5] M. Panjehpour, A. Wilke, D.L. Frazier, B.F. Overholt, Hyperthermia treatment using a computer controlled Nd:YAG laser system in combination with surface cooling, Proc. SPIE (1991) 307–315.
[6] F. Manns, P.J. Milne, X. Gonzalez-Cirre, D.B. Denham, J.M. Parel, D.S. Robinson, In-situ temperature measurements with thermocouple probes during laser interstitial thermometry (LITT): quantification and correction of a measurement artifact, Lasers Surg. Med. 23 (1998) 94–103.
[7] Z. Amin, J.J. Donald, A. Masters, R. Kant, W. Lees, S. Brown, Interstitial laser photocoagulation therapy for liver tumours: clinical results, SPIE Laser–Tissue Interact. IV 1882 (1993) 202–209.
[8] F.K. Storm, Hyperthermia in Cancer Therapy, Boston, 1983.
[9] G.M. Hahn, Potential for therapy of drugs and hyperthermia, Cancer Res. 39 (1979) 2264–2268.
[10] M.P. Fried, Lasers in clinical otolaryngology: current uses and future applications, Ear Nose Throat J. 70 (1991) 843–847.
[11] T.J. Vogl, M.G. Mack, R. Straub, A. Roggan, R. Felix, Percutaneous MRI-guided laser-induced thermotherapy for hepatic metastases for colorectal cancer, Lancet (1997) 329–350.
[12] T.J. Vogl, M.G. Mack, R. Straub, A. Roggan, R. Felix, Magnetic resonance imaging – guided abdominal interventional radiology: laser-induced thermotherapy of liver metastases, Endoscopy 27 (1997) 577–583.
[13] S.G. Brown, Phototherapy of tumor, World J. Surg. 7 (1983) 700–709.
[14] T. Shroder, J. Hahl, Laser induced hyperthermia in the treatment of liver tumours, Lasers Surg. Med. (Suppl. 1) (1989) A-53.
[15] S.T. Harms, H. Mumtaz, B. Hyslop, S. Klimberg, K. Westbrook, S. Kourourian, RODEO MRI guided laser ablation of breast cancer, Proc. SPIE (1999) 484–489.
[16] J. Wahrburg, K.U. Schmidt, A new system for minimal invasive ablation of deep seated brain tumors, Proc. IEEE/EMBS (1997) 2438–2441.

[17] T.G. Van Leeuwen, E.D. Jansen, M. Motamedi, C. Borst, A.J. Welch, Physics of laser induced hyperthermia, in: A.J. Welch, M.J.C. van Germet (Eds.), Optical-thermal Response of Laser-irradiated Tissue, Plenum, New York, 1995, pp. 789–829.
[18] S.W. Jeong, H. Liu, W.R. Chen, Temperature control in deep tumor treatment, Proc. SPIE (2003) 216–226.
[19] J. Feyh, R. Gutmann, A. Leunig, L. Jager, M. Reiser, R.E. Saxton, D.J. Castro, M.D. Kastenbauer, MRI-Guided laser interstitial thermal therapy (LITT) of head and neck tumors: progress with a new method, J. Clin. Laser Med. Surg. 14 (1996) 361–366.
[20] S.A. Sapareto, W.C. Dewey, Thermal dose determination in cancer therapy, Inter. J. Radiat. Oncol. Biol. Phys. 10 (1984) 787–800.
[21] D. Arora, M. Skliar, R.B. Roemer, Minimum-time thermal dose control of thermal therapies, IEEE Trans. Biomed. Eng. 52 (2005) 191–200.
[22] D.S. Robinson, J.M. Parel, D.B. Denham, X. Gonzalez-Cirre, F. Manns, P.J. Milne, R.D. Schachner, A.J. Herron, J. Comander, G. Hauptmann, Interstitial laser hyperthermia model development for minimally invasive therapy of breast carcinoma, J. Am. Coll. Surg. 186 (1998) 284–292.
[23] S. Zangos, M.G. Mark, J.O. Balzer, B.K. Engelmann, R. Straub, K. Eichler, C. Hergoz, T. Lehnert, O. Sollner, M. Heller, A. Thalhammer, T.J. Vogl, Neoadjuvant transarterial chemoembolization (TACE) before percutaneous MR-guided laser-induced thermotherapy (LITT): results in large-size primary and secondary liver tumors, Med. Laser Appl. 19 (2004) 98–108.
[24] M. Pech, G. Wieners, F. Fischbach, S. Hengst, A. Beck, G. Warschewske, E.L. Hanninen, P. Wust, J. Ricke, Synchronous CT-guided brachytherapy in patients at risk for incomplete interstitial laser ablation of liver malignancies, Med. Laser Appl. 19 (2004) 73–82.
[25] M.J.C. Van Gemert, A.J. Welch, Clinical use of laser–tissue interaction, IEEE Eng. Med. Biol. Mag. (1989) 10–13.
[26] L. Wang, X. Liang, P.A. Galland, P.P. Ho, R.R. Alfano, Detection of objects hidden in highly scattering media using time-gated imaging methods, Proc. SPIE (1999) 261–264.
[27] D. Manstein, G.S. Herron, R.K. Sink, H. Tanner, R.R. Anderson, Fractional photothermolysis: a new concept for cutaneous remodeling using microscopic patterns thermal injury, Lasers Surg. Med. 34 (2004) 426–438.
[28] M.H. Khan, R.K. Sink, D. Manstein, D. Eimerl, R.R. Anderson, Intradermally focused infrared laser pulses: thermal effects at defined tissue depths, Lasers Surg. Med. 36 (2005) 270–280.
[29] T. Gratzl, G. Dohr, H. Schmidt-Kloiber, E. Reichel, Histological distinction of mechanical and thermal defects produced by nanosecond laser pulses in striated muscle at 1064 nm, Proc. SPIE (1991) 55–62.
[30] D.D. Joseph, L. Preziosi, Heat waves, Rev. Mod. Phys. 61 (1989) 41–73.
[31] P.J. Antaki, New interpretation of non-Fourier heat conduction in processed meat, ASME J. Heat Transfer 127 (2005) 189–193.
[32] W. Kaminski, Hyperbolic heat conduction equation for materials with a nonhomogenous inner structure, ASME J. Heat Transfer 112 (1990) 555–560.
[33] K. Mitra, S. Kumar, A. Vedavarz, M.K. Moallemi, Experimental evidence of hyperbolic heat conduction in processed meat, ASME J. Heat Transfer 117 (1995) 568–573.
[34] W.R. Chen, Selective photothermal interaction using near-infrared laser and laser absorbing dye in gel phantom and chicken breast tissue, Proc. SPIE (2003) 18–25.
[35] J. Liu, X. Chen, L.X. Xu, New thermal wave aspects on burn evaluation of skin subjected to instantaneous heating, IEEE Trans. Biomed. Eng. 46 (1999) 420–428.
[36] Z.S. Deng, J. Liu, Analytical study on bioheat transfer problems with spatial or transient heating on skin surface or inside biological bodies, ASME J. Biomech. Eng. 124 (2002) 638–649.
[37] J.P.L. Huillier, Theoretical analysis of the role played by tissue-optical parameters in laser ablation process, Proc. SPIE (1997) 151–165.
[38] A. Banerjee, A. Ogale, C. Das, K. Mitra, C. Subramanian, Temperature distribution in different materials due to short pulse laser irradiation, Heat Transfer Eng. 26 (2005) 41–49.
[39] Z. Guo, S.K. Wan, K.H. Kim, C. Kosaruja, Comparing diffusion approximation with radiation transfer analysis for light transport in tissues, Opt. Rev. 10 (2003) 415–421.
[40] S.A. Boppart, J. Herrmann, C. Pitris, D.L. Stamper, M.E. Brezinski, J.G. Fujimoto, High-resolution optical coherence tomography-guided laser ablation of surgical tissue, J. Surg. Res. 82 (1999) 275–284.
[41] U. Hohenleutner, S. Hohenleutner, W. Baumler, M. Landthaler, Fast and effective skin ablation with an Er:YAG laser: determination of ablation rates and thermal damage zones, Lasers Surg. Med. 20 (1997) 242–247.
[42] J.I. Youn, P. Sweet, G.M. Peavy, V. Venugopalan, Mid-IR laser ablation of articular and fibro-cartilage: a wavelength dependence study of thermal injury and crater morphology, Lasers Surg. Med. 38 (2006) 218–228.
[43] A.M. Gobin, P. O'Neal, D.M. Watkins, N.J. Halas, R.A. Drezek, J.L. West, Near infrared laser–tissue welding using nanoshells an exogenous absorber, Lasers Surg. Med. 37 (2005) 123–129.
[44] J.K. Presnell, M.P. Schreibman, Animal Tissue Techniques, The Johns Hopkins University Press, Baltimore/London, 1997.
[45] M.F. Modest, Radiative Heat Transfer, second ed., McGraw-Hill, New York, 2003.
[46] K.H. Kim, Z. Guo, Ultrafast radiation heat transfer in laser tissue welding and soldering, Numer. Heat Transfer A 46 (2004) 23–46.
[47] M.N. Ozisik, D.Y. Tzou, On the wave theory of heat conduction, ASME J. Heat Transfer 116 (1994) 526–535.
[48] K.E. Glass, M.N. Ozisik, D.S. McRae, B. Vick, Hyperbolic heat conduction with temperature-dependent thermal conductivity, J. Appl. Phys. 59 (1986) 1861–1865.
[49] A. Vedavarz, K. Mitra, S. Kumar, Hyperbolic temperature profiles for laser surface interactions, J. Appl. Phys. 76 (1994) 5014–5021.
[50] K.H. Kim, Z. Guo, Multi-time-scale heat transfer modeling of turbid tissues exposed to short-pulsed irradiations, Comput. Meth. Prog. Biomed. 86 (2007) 112–123.
[51] C. Das, A. Trivedi, K. Mitra, T. Vo-Dinh, Experimental and numerical analysis of short pulse laser interaction with tissue phantoms containing inhomogeneities, Appl. Opt. 42 (2003) 5173–5180.
[52] P.L. Djorev, E. Borisova, L. Avramov, Interaction of the IR laser radiation with human skin – Monte-Carlo simulation, Proc. SPIE (2003) 403–407.
[53] R.C. Simpson, M. Kohl, M. Essenpreis, M. Cope, Near-infrared optical properties of ex vivo human skin and subcutaneous tissues measured using the Monte Carlo inversion technique, Phys. Med. Biol. 43 (1998) 2465–2478.
[54] K.N. Rai, S.K. Rai, Effect of metabolic heat generation and blood perfusion on the heat transfer in the tissues with blood vessels, Heat Mass Transfer 35 (1999) 75–79.
[55] S.L. Jacques, Skin Optics, Oregon Medical Laser Center News, 1998.